Electrophysiological events recorded at presynaptic terminals of the crayfish neuromuscular junction with a voltage indicator

Jen-Wei Lin

Biology Department, Boston University, Boston, USA

The water-soluble voltage indicator JPW1114 was used to stain thin axons and terminal varicosities of the crayfish neuromuscular junction. A slow, overnight injection protocol was developed to brightly stain fine structures without cytotoxicity. Fluorescence transients filtered at 2 kHz showed that the duration of terminal action potentials was shorter than that of those recorded in the main trunk of the axons. In addition, the repolarization phases of the terminal and axonal action potentials overlapped in time, suggesting that the entire axonal arborization repolarizes simultaneously. Manipulating resting membrane potential, ±15–20 mV, did not alter the peak level or duration of action potentials if they fired in isolation. A prolongation of action potential, by 23%, could be induced if a 10-spike burst at 100 Hz was fired from depolarized membrane potential. No such change was observed when the high frequency train was fired from resting or hyperpolarized levels. Microelectrodes in the main trunk of axons typically recorded a depolarizing after-potential (DAP) following an action potential initiated from resting membrane potential. The DAP could be inverted and enlarged by depolarization and hyperpolarization, respectively. Fluorescence transients recorded from terminals exhibited similar DAP characteristics. The ratio of DAP to action potential amplitude recorded from terminals was similar to that recorded from the main axon. Thus, the entire axonal arborization returned to resting level in a spatially uniform manner during the DAP. The functional significance of DAP is discussed in the light of these observations.

(Received 9 June 2008; accepted after revision 26 August 2008; first published online 28 August 2008)
Corresponding author J.-W. Lin: Biology Department, Boston University, 5 Cummington Street, Boston, MA 02215, USA. Email: jenwelin@bu.edu

Axon, soma and dendrites comprise the three structural components of a typical neuron. Excitability and synaptic interaction have been studied extensively in soma and dendrites due to the accessibility of these structures. In comparison, measurement of electrophysiological events in fine axonal branches has been relatively rare. Due to better accessibility, intra- and extracellular recordings of single axons in invertebrate preparations have contributed significantly to our understanding of signal processing in axons (Debanne, 2004). Mechanisms of axon-mediated signal processing include: branch point filtering (Grossman *et al.* 1979; Smith, 1980; Gu, 1991), action potential reflection-mediated synaptic facilitation (Baccus, 1998) and presynaptic modulation mediated through axo-axonic synapses (Dudel & Kuffler, 1961; Cattaert *et al.* 2001; see MacDermott *et al.* 1999 for review). However, even with the better accessibility of invertebrate preparations, microelectrode penetration of the fine axonal branches, necessary for precise electrophysiological observation, is still impractical.

In mammalian preparations, insights to the general question of electrophysiological activity in fine axons have been inferred by recording directly from synaptic terminals. For example, recording from terminal regions of the calyx of Held revealed the functional significance of Na^+ channel localization at the heminodal region proximal to the synaptic area (Leao *et al.* 2005). Modelling of mossy fibre boutons suggested that Na^+ channels in terminal varicosities are important for the amplitude of action potential at active zones whereas Na^+ channels in connecting axons mainly facilitate the propagation of an action potential (Engel & Jonas, 2005). In the posterior pituitary, the invasion of action potentials from thin connecting axons into varicosities was variable and subject to modulation (Wilke *et al.* 1998). Other less direct approaches have also been used to study branching axon excitability. For example, Ca^{2+} imaging studies

This paper has online supplemental material.

DOI: 10.1113/jphysiol.2008.158089

of terminal boutons or postsynaptic spines were used to investigate whether branch point failure actually occurs in single mammalian central axons (Cox *et al.* 2000; Koester & Sakmann, 2000). Extracellular field recording and stimulation were used to examine the role of I_h (a hyperpolarization activated cationic current) on terminal excitability in brain slices (Soleng *et al.* 2003). In some special cases, when neurons are electrotonically compact, somatic recording has been used to infer $GABA_A$ receptor-mediated activities in presynaptic terminals (Pouzat & Marty, 1999; Mejia-Gervacio & Marty, 2006).

One of the few possible alternatives enabling circumvention of difficulties related to microelectrode accessibility is the use of a voltage indicator. Although there has been considerable success in using voltage-sensitive dye to study soma-dendritic signal processing at a single cell level (Djurisic *et al.* 2004; Palmer & Stuart, 2006), the low mobility of voltage indicators makes it hard to stain axons of great length or with extensive branching. In this report, a water-soluble variant of the voltage indicator JPW1114 is used to achieve bright staining in a single axon of the crayfish opener neuromuscular preparation.

Methods

Preparation and electrophysiology

Crayfish, *Procambarus clarkii*, were obtained from Atchafalaya Biological Supplies (Raceland, LA, USA). Animals, ∼4 cm head to tail, were maintained in tap water at room temperature (22°C) and fed three times per week, with water replaced after feeding. All experiments were performed at room temperature. The opener muscle of the first walking leg was used for all experiments. The leg was first removed by autotomy and glued to a 15 mm Petri dish with Crazy glue. The opener axon muscle preparation was then dissected in saline. Physiological saline contained (in mM): 195 NaCl, 5.4 KCl, 13.5 $CaCl_2$, 2.6 $MgCl_2$ and 10 Hepes, titrated to pH 7.4 by NaOH. Glucose (1 mg ml^{-1}) and gentamicin (1 μg ml^{-1}) were added to the saline during overnight injection. Microelectrodes used to record the presynaptic axon contained 250 mM potassium methanesulphonate and 250 mM K-Hepes (40 MΩ). The typical resting membrane potential was ∼ −70 mV, and preparations with resting level less than −65 mV were not included in this report. All chemicals used to make up the saline were purchased from Sigma. Gentamicin was purchased from Gibco. JPW1114 was purchased form Invitrogen (D6923).

Photometric measurement of fluorescence transients

Photometric measurement of fluorescence transients in this preparation has been previously described (Vyshedskiy & Lin, 2000). Briefly, a photodiode (S5973-01; Hamamatsu, Bridgewater, NJ, USA) was used to record fluorescence transients on an upright microscope (Axioskop; Zeiss, Oberkochen, Germany) with a ×40 or ×60 water immersion lens. The photocurrent was measured using a single channel head stage, coupled to Geneclamp 500. A 150 W xenon lamp, in a 770 Lamphouse (Optiquip), was driven by an Optiquip 1600 power supply. The filter set used for JPW1114 fluorescence transients included: excitor 525/45 band-pass filter; dichroic 560 nm long pass and emitter 575 nm long pass. Illumination was gated by a shutter (Uniblitz; Vincent Associates) mounted to the legs of the vibration isolation table, uncoupled from the lamp house and microscope to avoid mechanical artifacts picked up by the photodiode. The area of illumination was restricted by an iris diaphragm customized to allow an illumination diameter of 20–50 μm with a ×60 objective. Normalization of fluorescence transients was calculated as $\Delta F/F = (F(t) - F_{rest})/F_{rest} \times 100$, where F_{rest} represents the fluorescence intensity of stained varicosities in the absence of activity. Background fluorescence in unstained regions was not subtracted.

Most voltage indicators are highly lipophilic and are typically dissolved in organic solvents first before being dispersed in saline for extracellular staining. In order to selectively stain a single axon with a voltage-sensitive dye, intracellular injection of a water-soluble voltage indicator JPW1114 was the reagent of choice. There are two main difficulties when using this indicator: (1) being able to inject a sufficiently large quantity to achieve good staining, and (2) avoiding toxicity associated with high concentrations. In addition, the slow spread of JPW1114 fluorescence suggests that this dye partitions into the membrane near its injection site, a condition that exacerbates local toxicity if a large quantity is injected in a single bolus. To avoid high concentrations locally and yet inject a sufficient quantity, I found it best to repeat small injection steps at a slow rate but over an extended period. A protocol was developed where injection started around 5 pm and continued overnight. After impaling an axon with a dye-containing electrode, the indicator was injected in 3 nA–800 ms steps repeated once every minute. The 3 nA step was alternated with a −3 nA step of the same duration, also once per minute, to keep the electrode clear. With this protocol, axons were typically well stained and viable next morning. The injection microelectrode stayed intracellular over this period in most cases.

The JPW1114 injection pipette was first backfilled by dipping the back end of the microelectrode in the dye solution, which contained JPW1114 (0.5 mg ml^{-1}), potassium methanesulphonate (330 mM), K-Hepes (2 mM) and K-GABA (250 mM). Hepes and GABA salts were included to maintain pH and improve viability, respectively. After all the dye solution had moved

to the tip by capillary action, the electrode was back-filled by briefly dipping in a solution containing 1 M potassium methanesulphonate and 5 mM K-Hepes.

Comparing the waveforms of fluorescence transients with microelectrode recordings

A typical experimental configuration is shown in Fig. 1*A*. The indicator injection site (I) was located at the branch point where secondary branches (2°) emerged from the primary (1°) axon. In all experiments, a second voltage-recording electrode was positioned at a secondary branch where a tertiary branch emerged (V). The image shown in Fig. 1*A* was acquired 16 h after the start of indicator injection, by which time the staining was distributed to all axon branches exposed for observation, ∼2.5 mm. In this particular preparation, the inhibitor was strongly stained (lower branch) whereas the excitor (upper branch) was weakly stained. Preparations remained viable up to 48 h, as judged by excitability and synaptic transmission. Recordings of local activity were obtained by closing the field diaphragm in the epifluorescence light path to restrict the area of illumination. A typical circular area of fluorescence illumination had a diameter of 30–50 μm and contained a cluster of approximately five varicosities (Fig. 1*A* dashed circle and inset). To optimize

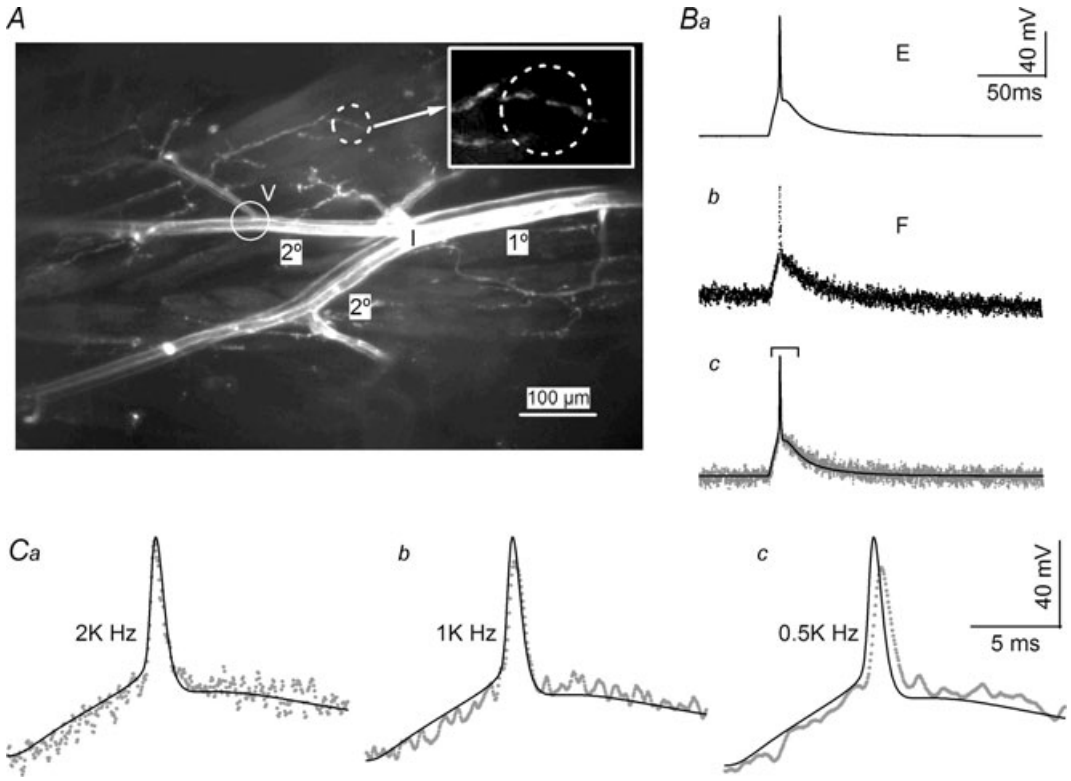

Figure 1. Accuracy of fluorescence transients reported by JPW1114
A, stained presynaptic axons after overnight injection. Both excitor, upper, and inhibitor, lower, were stained in this preparation but the latter was more brightly labelled. The location of dye injection (I) was at the branching point where the primary axon (1°) gave rise to two secondary branches (2°). The typical location for the second voltage-recording microelectrode was located near a point where a tertiary branch emerges (V). The dashed circle identifies a typical area where the fluorescence signal of a presynaptic terminal would be recorded, see inset for details. The image was obtained by collapsing 30 confocal stacks collected with a ×10 water lens. The inhibitor was injected for 15 h and the excitor for 3 h. *Ba*, microelectrode recording (E trace) of an action potential obtained from the preparation shown in *A*. The action potential was evoked by a 10 ms current step delivered through the current electrode at the main branching point (I). *Bb*, the fluorescence transient (F trace) recorded simultaneously with the E trace shown in *Ba*. The location of the imaging site was the same as the location of the voltage electrode. Traces in *Ba* and *b* are averages of 12 traces. *Bc*, superimposition of the E and F traces. A linear trend has been subtracted from the F trace to remove the decline due to dye bleaching. Both E and F traces have been aligned before averaging; see Fig. 4*B* for details of trace alignment. *Ca*, expanded traces identified in the bracket in *Bc*. The action potentials of E and F traces exhibit identical time courses, confirming the fidelity of the voltage indicator. *Cb* and c, F traces recorded under indicated filtering before data digitization. Although 1 and 0.5 kHz filtering significantly reduced baseline noise levels, the procedure clearly slowed and truncated the action potential waveform.

the correlation between microelectrode recordings and fluorescence transients, only terminals distal to the voltage electrode were chosen for imaging studies.

The fidelity of the fluorescence transient was first verified by comparing the time courses of microelectrode recordings (E) and fluorescence transients (F) obtained from the same location (Fig. 1*A*, circle near the V). An action potential was activated by a 10 ms current step (Fig. 1*Ba*). Due to photobleaching, a slight declining trend in the simultaneously recorded fluorescence transient could be detected (Fig. 1*Bb*). After correcting for bleaching by subtracting a linear trend, the superimposed E and F traces showed a perfect match for potentials before and after the spike (Fig. 1*Bc*). Detailed comparison of action potentials is shown on an expanded time scale in Fig. 1*Ca*, again with a nearly perfect match. It should be noted that, due to the rapid time course of the action potential, excessive filtering of the fluorescence signal was not appropriate. For example, 1 or 0.5 kHz filtering of F traces resulted in reduced spike amplitude and delayed onset (Fig. 1*Cb* and *c*). Therefore, fluorescence transients were low-pass filtered at 2 kHz before being digitized at 50 μs. No further digital smoothing was used for action potential analyses.

Stability of the fluorescence transients

Due to significant bleaching of the voltage indicator, the stability of the action potential time course and amplitude was examined. An image of terminal varicosities with connecting axons is shown in Fig. 2*A*, where staining is clearly membrane specific. The area enclosed by the circle represents an imaged region where terminals are pale due to deliberate photobleaching. The identity of the globular structure in the varicosities in the lower branch remains to

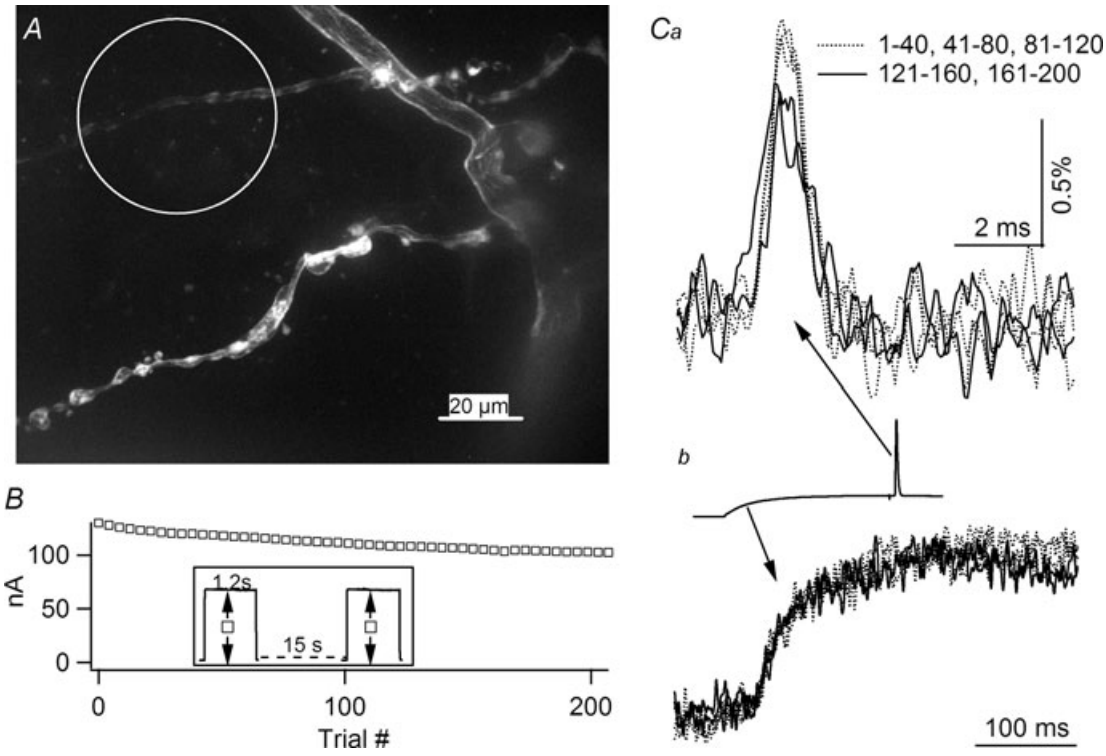

Figure 2. Light-induced toxicity is specific to action potentials
A, fine branches stained with JPW1114. The terminal branch enclosed in the circle has been deliberately bleached, 800 s total exposure, for visual identification. An unbleached terminal branch below the circle is typical of a well-stained cluster chosen for imaging. This image is a Z-projection stack of 30 confocal images collected with a ×40 water immersion lens. *B*, decline in the background fluorescence level during repeated exposure of the bleached branch shown in *A*. The *X*-axis indicates the exposure number while the *Y*-axis represents the current reading from a photodiode. Inset: experimental protocol showing 1.2 s shutter opening and 15 s gap between each exposure. Arrows emanating from open squares indicate the amplitude of the background fluorescence. *Ca*, normalized and averaged action potentials from 40 consecutive trials. The first three averages are identical in amplitude but the next two averages, 121–160 and 161–200, exhibit lower amplitudes. *Cb*, subthreshold responses, averaged from the same traces as those used in *Ca*, exhibit no degradation in signal amplitude. Inset: an example of a trace from which the action potentials in *Ca* and the subthreshold responses in *Cb* were obtained. The line styles in *Ca* and *Cb* are identical.

be further investigated. Figure 2*B* shows the fluorescence intensity recorded from the cluster of terminals within the circle in Fig. 2*A*. The inset shows that each trial involved an exposure time of 1.2 s with a 15 s gap between trials. The fluorescence level declined to 78% of its initial value after 200 consecutive exposures. The amplitude and time course of normalized action potentials averaged from 40 consecutive trials show that action potential amplitude remained constant for up 120 trials (Fig. 2*Ca*). Analysis of four additional preparations with shutter opening times of 0.6–1.2 s consistently showed that normalized action potential amplitude remained stable for a total exposure time of up to 120 s. The degradation seemed to be specific to action potentials, since normalized subthreshold transients evoked by current steps averaged from the same traces did not show detectable degradation (Fig. 2*Cb*). (See inset for the relative timing of the action potential and the subthreshold step.) Note that the illumination duration for individual trials in this example was unusually long, 1.2 s. Experiments using 100–200 ms shutter duration showed stable action potential amplitude for 500 exposures. It should also be noted that other clusters of terminals in the same preparation unexposed to illumination could still be used for further experiments.

Fluorescence signal calibration and resolution

In order to calibrate the fluorescence transients of voltage indicators, the relative amplitudes of action potentials and subthreshold responses of E and F traces were analysed in detail. Figure 3*A* shows the E trace from a secondary branch superimposed with F recordings from the cluster of terminals identified in Fig. 2*A*. The traces include a train of 10 action potentials at 100 Hz, fired during a hyperpolarizing current step, followed by passive voltage transients near the end, due to the termination of the current step. The two epochs are expanded in Fig. 3*Ba* and *b*, after subtracting the sloping trend due to photobleaching. (See Fig. 1 in Supplemental material for traces displayed without superimposition.) Here, the F traces of the two epochs have been scaled by a scaling constant to match the waveform of their corresponding E traces. This scaling constant for the action potential epoch was 3333 and the constant for the passive transient was 6863, with a ratio of 0.49 (R_{sc}). (The scaling constant was determined by factors such as the extent of staining, the area of imaging, the intensity of the light source and the amplification of the photocurrent. These factors are assumed to be constant within individual traces.) The larger scaling constant for the passive transient suggests that it has decayed in amplitude more than the action potential. In order to estimate the amplitude of electrophysiological events in the terminals, the peak of an action potential is assumed to reach a constant level throughout all locations of the axon. This assumption is in part supported by the observation that a shift in axonal membrane potential modifies the amplitude but not the peak level of action potentials (see Fig. 5 below). Figure 3*A* shows the action potential amplitudes of E and F traces labelled as AP_E and AP_F, respectively. The passive transients due to the current step in the axon and terminals are labelled as DC_E and DC_F. Taking into account the ratio of the scaling constants for action potential and subthreshold signals, these parameters should have the following relationship:

$$\frac{DC_F}{DC_E} = \frac{AP_F}{AP_E} \times R_{SC} \quad (1)$$

AP_E and DC_E are 82 and 17 mV, respectively, in this example. R_{SC} is 0.49. Thus, eqn (1) could be rewritten and expressed in terms of DC_F alone.

$$\frac{DC_F}{17} = \frac{(82 - (17 - DC_F))}{82} \times 0.49$$

DC_F thus solved is 7.4 mV and AP_F is 74.5 mV. Therefore, subthreshold signals decayed from 17 mV to 7.4 mV, namely by 56%, while action potential amplitude was only slightly reduced, by 9%, because it was riding on a less hyperpolarized membrane potential. Although the decay of passive responses was not surprising, the time constants of the E and F transients were very similar, showing little sign of spatial filtering (Fig. 3*Bb*). Based on the same estimating procedure, averaged results from seven preparations showed that subthreshold signals decayed to $75 \pm 8\%$ of those measured with microelectrodes at the junction between secondary and tertiary branches. The variation was presumably due to differences among preparations in the distance between the V electrode and imaging sites.

Recordings shown here also provide an assessment of the resolution of fluorescence recordings in terminals. The standard deviation of the baseline noise level for the F trace was 2.7 mV. Therefore, assuming that detectable signals should be larger than 3 times the baseline standard deviation, the minimal signal detectable at 2 kHz filtering would be ~9 mV. This resolution was improved by digital smoothing for signals with a slower time course. For example, when the F traces for the passive transient shown in Fig. 3*Bb* were processed with binomial smoothing, 100 points, the 3 × baseline standard deviation decreased to ~4 mV.

Since the duration of an action potential is essential for controlling the amount of Ca^{2+} influx, it was important to measure this parameter objectively. A Gaussian function was used to obtain a best fit to the main body of an action potential, excluding slow components immediately before and after the spike. The Gaussian function was chosen because of the relatively symmetrical waveform of action potentials in this preparation (see Fig. 1*Ca*). The half-width of the Gaussian curve was calculated as $\sigma \times 2.355$

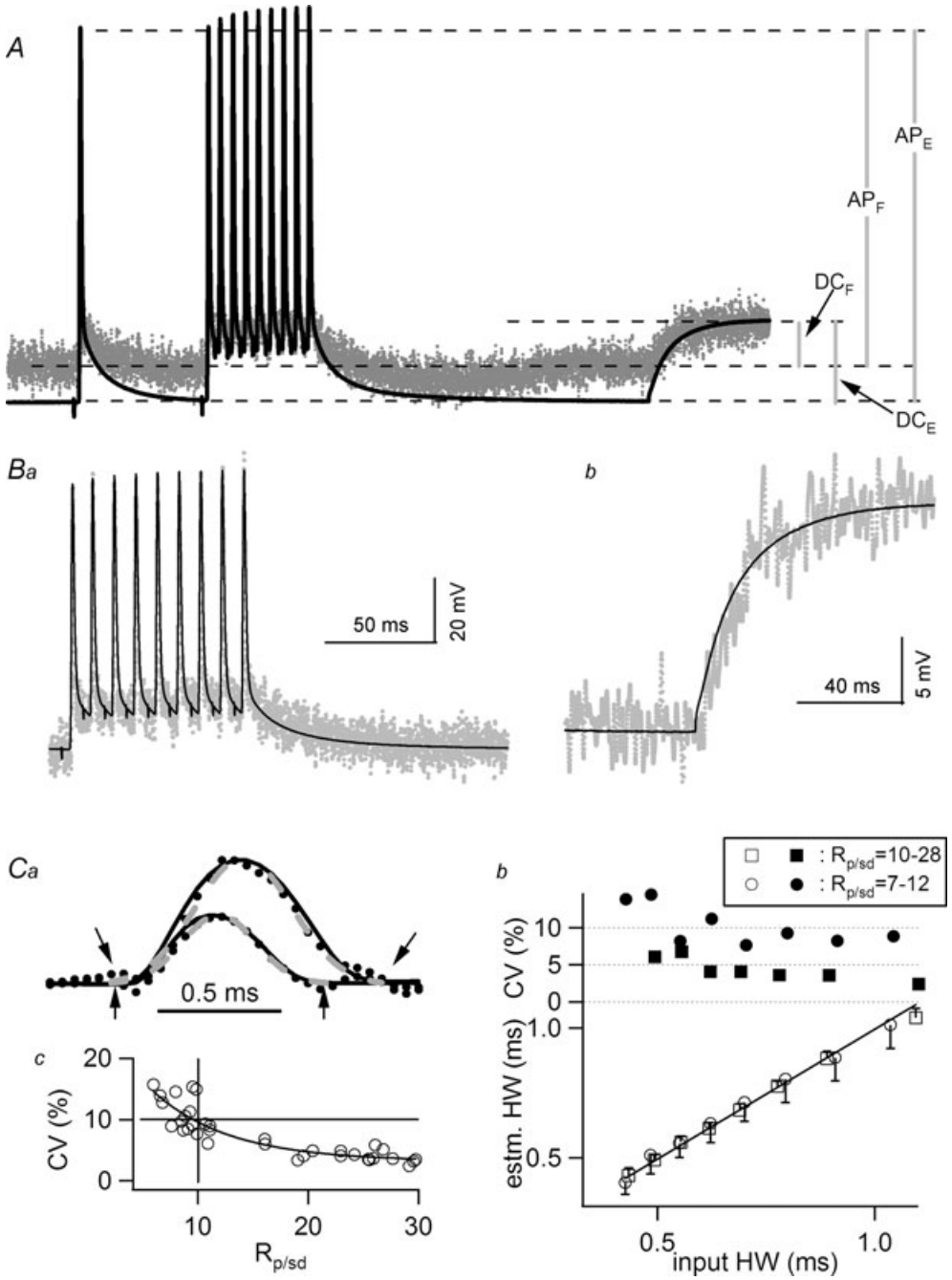

Figure 3. Calibration of fluorescence signals measured in presynaptic terminals
A, F traces recorded from the cluster of terminals circled in Fig. 2*A*. The E trace was recorded simultaneously. Action potentials, a single one followed by a train fired at 100 Hz, were initiated during a hyperpolarizing current step. Termination of the current step led to the passive rise near the end of the traces. The two traces are aligned in time but the *Y*-axes are scaled for the convenience of illustrating various components of measurement. AP_E and AP_F represent the amplitudes of action potential recorded with E and F traces, respectively. DC_E and DC_F represent subthreshold responses arising from termination of a hyperpolarizing current step. *Ba*, superimposed E and F traces obtained during the 100 Hz train shown in *A*. The F trace has been scaled to provide the best fit to the E trace, with a scaling constant of 3333. The best fit was determined visually such that the peaks of action potentials, baseline and the depolarizing after-potential all overlap. *Bb*, superimposed E and F traces obtained during the subthreshold response. The F trace, with a scaling constant of 6863, has been binomially smoothed, 100 points, to better illustrate signals with smaller amplitude. Both E and F traces were averaged from 25 traces. *Ca*, action potential-like LED transients were used to assess the reliability of action potential half-width estimates. Two examples of LED transients (dotted lines), with signal-to-noise ratios of 20 and 12, respectively, are superimposable with the input LED emission recorded with minimal noise (continuous lines). (See text for details

where σ represents standard deviation. An empirical approach was used to evaluate the accuracy of this procedure. An LED was driven by a series of Gaussian-like waves with increasing half-width from 0.4 to 1 ms. These waveforms were obtained by feeding a series of trapezoid waves through a low-pass filter set at 500 Hz. The trapezoid waves were 4 V in amplitude with rising and decay times of 0.1 and 0.2 ms, respectively, and the plateau duration was varied from 0.4 to 1 ms in 0.1 ms steps. Examples of the resulting LED emission are shown in Fig. 3*Ca* (continuous curves). In order to simulate experimental conditions, the intensity of the LED emission was reduced by moving it away from the microscope objective such that the signal-to-noise ratio of LED transients, measured with the JPW1114 filter set in place, approximated experimental data. When a JPW1114 transient was zeroed and then divided by the standard deviation of its baseline, the action potential peak level ranged from 7 to 30 ($R_{p/sd}$). For example, the F trace in Fig. 3*A* has a $R_{p/sd}$ value of 23. Figure 3*Ca* shows two examples of LED transients, each an average of 20 traces, with $R_{p/sd}$ of 20 and 12, respectively (dotted curves). The time courses of 'realistic' LED transients overlap with the LED emission (continuous curves). Gaussian fits to these LED transients are also displayed (Fig. 3*Ca*, dashed grey curves). (Arrows identify the region of the curve fits.) In the lower panel of Fig. 3*Cb*, half-widths estimated from the Gaussian fits were plotted against the input half-widths for a series of durations where the $R_{p/sd}$ ratio ranged from 10 to 28 (□). The data points follow the 45 deg line, suggesting accurate recovery of input half-widths. Each data point was averaged from 10 trials and each trial was averaged from 20 traces. Thus, each trial was equivalent to the half-width estimated from one terminal cluster. For example, the F trace in Fig. 3*A* would yield one of the 10 values used to calculate the average for one data point in this plot. The coefficients of variation from this series of tests were mostly less than 5% (upper panel, ■). When the simulated $R_{p/sd}$ ratio was lowered to a 7–12 range, the recovered half-widths were still accurate (○) but the coefficients of variation (●) were higher, $> 5\%$. The relationship between the coefficients of variation of the recovered half-widths and $R_{p/sd}$ ratios exhibited a clear negative correlation (Fig. 3*Cc*). In order to keep the coefficient of variation below 10%, only experiments with $R_{p/sd}$ values above 10 were used in this report. Furthermore, when half-widths from different preparations were compiled, the average was weighted by the $R_{p/sd}$ of each preparation. Thus, experiments with good signal-to-noise ratios were weighted more heavily in the averages.

All averaged results are presented as mean ± standard error of means unless indicated otherwise.

Results

Waveform of action potentials in the presynaptic terminal

One of the main objectives of this study was to examine in detail the waveform of action potentials at terminal varicosities. Figure 4*A* shows superimposed F traces recorded from a secondary axon (continuous line) and from a cluster of terminals (dashed grey line) in the same preparation. (To maintain consistency in data filtering characteristics, direct comparison between F traces is used here.) The F trace recorded from terminals showed a delayed rising phase due to a conduction lag (Fig. 4*Aa* and *b*). In addition, the falling phases of the two action potentials overlapped and the duration of the terminal action potential was shorter (Fig. 4*Ab*). Aligning the rising phases of the two traces showed that axonal and terminal action potentials exhibited a similar rate of rise but the latter repolarized more rapidly (Fig. 4*Ac*). Thus, it appears that the falling phase of action potentials in the main trunk is shaped in part by the antidromic spread of terminal activities. The action potentials shown in the panels in Fig. 4*A* were evoked by current steps, under two-electrode current clamp, from resting membrane potential. Since action potentials thus activated exhibited a variable onset, the F traces had to be aligned before averaging. Figure 4*B* illustrates the alignment procedure. The maximal point of the derivative of an E trace was first located (Fig. 4*Bb*, arrow) and a defined number of data points before and after the maximum were then duplicated into a new file for averaging. F traces recorded simultaneously were then 'cut out' with the same data point indexing. F traces

on the generation of these traces and the definition of signal-to-noise ratio ($R_{p/sd}$)). Also shown are the Gaussian fits to the LED transients (dashed grey lines). Downward (upward) arrows mark the time window of the Gaussian fit to the LED transient with an $R_{p/sd}$ value of 20 (12). *Cb*, lower panel: half-widths recovered from Gaussian fits plotted against half-widths of the corresponding input LED emission. Each data point, with standard deviation for its error bar, is the average of 10 trials and each trial is an average of 20 traces. Recovered half-widths match those of the input transients perfectly. The coefficient of variation calculated from each point is displayed on the upper panel. The squares represent LED transients with an $R_{p/sd}$ value between 10 and 28, whereas the circles were calculated from a separate series with an $R_{p/sd}$ range of 7–12. *Cc*, correlation between the coefficient of variation of recovered half-widths and the $R_{p/sd}$ of the LED transients from which half-width estimates were calculated. The vertical and horizontal lines highlight that in order to keep the coefficients of variation of the estimated half-width under 10%, the $R_{p/sd}$ value should be at least 10.

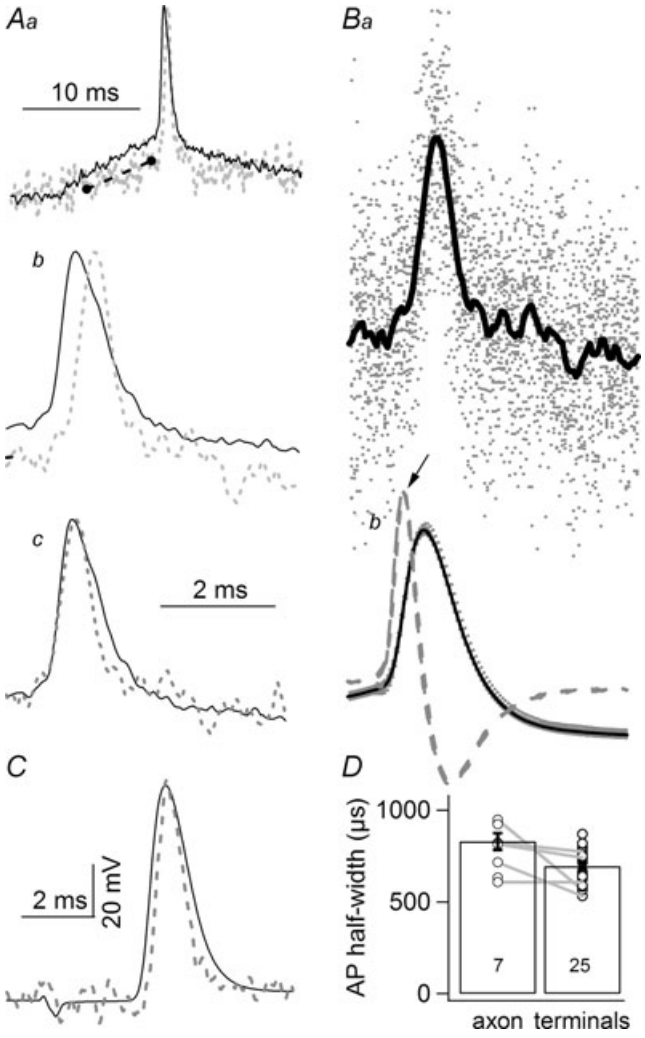

Figure 4. The duration of action potentials in terminal branches is shorter than that recorded in the main branches of axons
Aa, superimposed F traces recorded from the secondary axon (continuous line), same location as the V electrode, and terminals (dashed grey line) of the same preparation. The action potential was evoked by a current injection step from resting membrane potential. Both traces are the average of 22 traces. The black dashed line marks the shallower slope of the rising phase of the terminal recording as compared to that of the axonal recording, indicating spatial decay of the subthreshold signal. Note that both traces are fluorescence transients, to ensure identical filtering characteristics of the recordings. *Ab*, action potentials shown in *Aa* are displayed on an expanded time scale. The two action potentials cross each other in their falling phases but the terminal action potential exhibits a later onset, due to conduction delay. *Ac*, the two action potentials shown in *Ab* are normalized and aligned in their rising phase, to better demonstrate the reduced duration of the terminal action potential. All traces in *A* are in arbitrary units, not shown. *Ba* and *b*, an illustration of the alignment procedure. *Ba*, individual F traces, dotted ($n = 24$), and the average calculated from these traces (continuous line) are superimposed. These traces have already been aligned. *Bb*, superimposed action potentials recorded with a microelectrode. Two action potentials are shown using different symbols. Dashed traces represent derivatives of the E traces. One thousand data points, at 50 μs sampling, before and 2000 points after the maximum (arrow) were then duplicated into a new file for data averaging. The same data point indexing was used for duplication and averaging of F traces recorded simultaneously. *C*, another example of action potential comparison between an E trace recorded in the secondary axon and the corresponding F trace recorded in the terminals. In this case, action potentials were evoked by suction electrode stimulation. The characteristic narrower terminal action potential is also present. Therefore, the shorter duration of the terminal action potential is independent of the method used to initiate the action potentials. *D*, comparison of axonal and terminal action potential half-widths. The duration of action potentials measured in terminals is significantly ($P < 0.01$, Student's *t* test) shorter than the duration of those recorded in secondary axons. Only fluorescence transients, not E traces, were included when averaging axonal half-widths. Numbers in histogram columns are sample sizes.

from individual trials are shown (grey dots) with the superimposed average trace (continuous line; $n = 24$) in Fig. 4*Ba*. A terminal F trace obtained from a different preparation where action potentials were evoked by suction electrode stimulation, also exhibited a narrower duration in the terminal (Fig. 4*C*). The averaged half-width of the terminal action potential was 695 ± 16 μs ($n = 25$), significantly shorter than that recorded in the axon ($P < 0.01$), which was 830 ± 45 μs ($n = 7$) (Fig. 4*D*). Additionally, in five preparations where action potential transients were recorded in both axons and terminals, the duration of the latter was consistently shorter (Fig. 4*D*, connected data points).

The ascending phase before the upstroke of the terminal action potential exhibited a significantly shallower slope than that recorded in the main axon (Fig. 4*Aa*, dashed line) if axonal and terminal recordings were aligned by the baseline and the peak of action potentials. The shallower slope of the terminal recording is consistent with the spatial decay of subthreshold signals.

Modulation of action potential by resting membrane potential

Axons of the crayfish opener preparation have been shown to express I_h and the modulation of this current can shift resting membrane potential by up to 10 mV (Dixon & Atwood, 1985; Beaumont & Zucker, 2000). In addition, it has been shown that depolarizing resting membrane potential in the main axon can increase transmitter release at this preparation (Wojtowicz & Atwood, 1984). Here I examined the possibility that this modulation could be due to a change in spike duration regulated by resting membrane potential.

Action potentials recorded at the three levels of membrane potential (resting, depolarizing and hyperpolarizing) were first compared (Fig. 5*A*, inset). A depolarizing after-potential (DAP) recorded at resting level was inverted by depolarization and enhanced by hyperpolarization (Fig. 5*A*, arrows). These characteristics were observed in both the main axonal branches,

E traces (continuous lines), and terminals, F traces (dotted grey lines). Detailed comparisons of action potentials recorded from each resting membrane potential are shown in Fig. 5*B*. The peak levels of E trace action potentials (Fig. 5*Ba–d*, dotted lines) remained constant despite a 30 mV difference in resting levels. When the baseline and DAP of F traces were scaled to match those of the E traces, their peak levels also remained constant (Fig. 5*Ba–c*). Therefore, shifting resting membrane potential resulted in no detectable change in the peak level of a terminal action potential and was accompanied by a corresponding change in action potential height measured from baseline to peak.

Superimposing F traces recorded from the three distinct resting levels revealed no detectable differences in the duration of terminal action potential despite a 30 mV difference in their baselines (Fig. 5*Bd*). The absence of resting potential-mediated modulation was also observed after a prolonged shift in resting level. A 5 s hyperpolarizing pre-pulse, sufficient to activate an I_h-mediated 'sag' (Fig. 5*Ca*, arrow), did not alter the duration of the action potential (Fig. 5*Cc*). Similarly, a 15 mV–5 s-long depolarizing pre-pulse did not alter terminal action potential duration either. Results from this series of studies were summarized by plotting the half-widths of action potentials against the resting membrane potentials

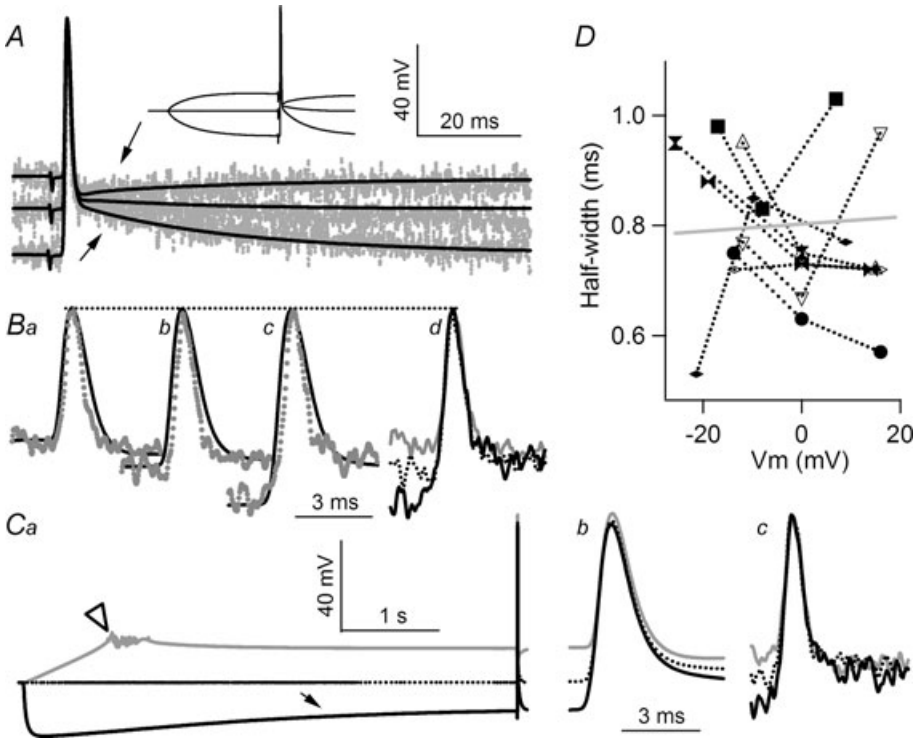

Figure 5. A shift in resting membrane potential does not modulate action potential duration
A, action potentials evoked by suction electrode stimulation were delivered during resting, depolarizing and hyperpolarizing resting membrane potentials, inset. Superimposed E (continuous lines) and F (dotted) traces show that the DAP could be inverted or enlarged (arrows) and is detected in both E and F traces. *Ba–c*, superimposed E and F traces of action potentials recorded from depolarized, resting and hyperpolarized membrane potential, respectively. The dashed line highlights that the peak of action potential is not affected by resting level of membrane potential. *Bd*, superimposed F traces of action potential showing that the duration of action potentials is not affected by the levels from which action potentials take off. *Ca*, test of action potential modulation by prolonged pre-potentials. The axon was depolarized by an initial ramp to minimize firing, although action potentials did occur in some traces (open arrowhead). Prolonged hyperpolarization activated an I_h-mediated sag (arrow). E (*Cb*) and F (*Cc*) traces of action potentials displayed on an expanded time scale show no modulation in action potential duration as a result of the prolonged conditioning. *D*, half-widths of action potentials measured in terminals do not correlate with resting membrane potential recorded in the secondary branch. The correlation coefficient of all data points (24) is 0.054 and is insignificant ($P > 0.5$). Zero on the *X*-axis represents resting membrane potential. Data points measured from the same terminals are connected, and each terminal is represented by a different symbol. Open symbols were obtained from experiments where prolonged, 5 s, prepulses were used. Traces in *A* and *B* share the same vertical scale. All traces in *C* share the same vertical scale. All recordings in this graph were obtained from the same preparation and were all averaged from 20 traces.

from which they were initiated, eight terminals in six preparations (Fig. 5*D*). There was no significant correlation between the two parameters, suggesting the absence of membrane potential-mediated modulation of action potential duration.

Frequency-dependent modulation of action potential waveform

The crayfish opener preparation has been used extensively as a model system for the analysis of synaptic facilitation (Zucker, 1974*a*; Dudel *et al.* 1983; Zucker & Regehr, 2002; Matveev *et al.* 2004). However, it has not been possible to determine whether frequency-dependent modulation of action potential duration at release sites contributes to the magnitude of synaptic facilitation. This issue was examined here. E and F traces during a 100 Hz train recorded at resting membrane potential are shown in Fig. 6*Aa*. Action potentials following the first one in the train took off from a slightly depolarized level due to a small but non-accumulating DAP (Fig. 6*Aa* and *b*). (The dashed horizontal line across the upper panels marks the resting membrane potential.) The 10th action potential exhibited slightly slower rising and falling phases than the first one (Fig. 6*Ab*, grey dotted trace) when the baselines of the two E traces were aligned. However, this small difference could not be resolved with confidence in the F traces due to their higher noise level (Fig. 6*Ac*). On average, the half-widths of the 1st and 10th action potentials were 760 ± 23 μs and 772 ± 31 μs, respectively, and were not statistically different ($n = 6$, $P > 0.5$).

Frequency-dependent modulation was also examined at depolarized and hyperpolarized membrane potentials. Due to the inversion of DAP at depolarized membrane

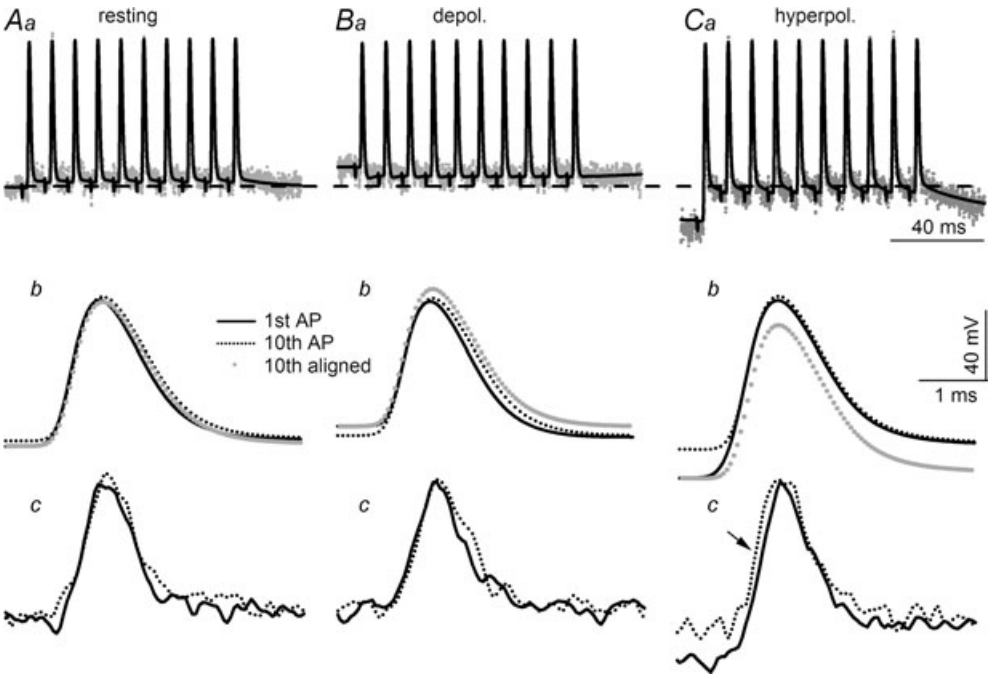

Figure 6. Modulation of action potential duration by high frequency firing
Ten action potentials were fired at 100 Hz initiated from resting (*Aa*), depolarized (*Ba*) and hyperpolarized (*Ca*) membrane potential. The horizontal dashed line across *Aa*, *Ba* and *Ca* represents resting level. Superimposed 1st and 10th action potentials recorded with a microelectrode in the secondary branches are shown for resting (*Ab*), depolarized (*Bb*) and hyperpolarized (*Cb*) membrane potentials. The grey dotted trace is the 10th action potential aligned with the baseline of the 1st action potential. There is a clear increase in the amplitude and duration of the 10th action potential if the 100 Hz train is fired from a depolarized level (*Bb*). Due to the large amplitude of the DAP, the 1st action potential of the train fired from a hyperpolarized level is significantly larger than the 10th but there is no visible difference in duration (*Cb*). Superimposed 1st and 10th action potentials recorded from terminals are displayed for resting (*Ac*), depolarized (*Bc*) and hyperpolarized levels (*Cc*). Consistent with observations of E traces in *Bb*, the 10th terminal action potential recorded at a depolarized level also exhibits a noticeable increase in duration (*Bc*) but a difference in amplitude cannot be resolved. The amplitude of the leading action potential of the train fired from a hyperpolarized potential is visibly larger than the 10th (*Cc*) but there is no statistical difference in duration, see text. The arrow in *Cc* indicates an earlier arrival time for the 10th compared with the 1st action potential in the terminals. All recordings were obtained from the same terminal cluster and traces were averaged from 30 traces. All E traces use the same vertical calibration and all F traces are in arbitrary units but are scaled by a common factor.

potential, all action potentials following the first one in the train took off from a less depolarized level (Fig. 6*Ba* and *b*). In addition, the peak level of the 10th action potential was slightly higher in the E trace and, in conjunction with a less depolarized baseline, resulted in a notably greater amplitude for the last action potential (Fig. 6*Bb*). This difference is better illustrated by aligning the baselines of the 1st and 10th action potentials (Fig. 6*Bb*, grey dotted trace). The difference in amplitude was hard to resolve in the F traces (Fig. 6*Bc*). (Note that the techniques used in this report cannot resolve a difference of less than 10 mV for fast signals.) However, the duration of the 10th spike was visibly longer in the E trace (Fig. 6*Bb*) and this difference was also discernable in the F trace (Fig. 6*Bc*). Averaged results for the 1st and 10th action potentials recorded at depolarized membrane potential were 702 ± 30 μs and 863 ± 43 μs, respectively, and the difference was statistically significant ($n = 6$; $P < 0.05$).

When action potentials were activated during hyperpolarization, DAP was large such that the 10th action potential took off from a level ~15 mV more depolarized than the 1st one (Fig. 6*Ca*). However, the main body of the two action potentials overlapped almost perfectly (Fig. 6*Cb*, black continuous and dotted lines). When the baselines of the two action potentials were aligned, the 1st action potential exhibited a higher amplitude than the nine that followed it (Fig. 6*Cb*, grey dotted trace). Similar characteristics were also apparent in the F traces (Fig. 6*Cc*). On average, the half-widths of the 1st and 10th action potentials were 784 ± 28 μs and 799 ± 11 μs, respectively, and are statistically indistinguishable ($n = 6$, $P > 0.5$). Also note that there was a detectable reduction in the conduction time for the last action potential (Fig. 6*Cc*, arrow). The earlier arrival of the 10th action potential was presumably due to its conduction at a more depolarized level than the first spike. However, this difference in conduction time was not consistently resolved in all preparations.

Finally, high frequency bursts were also tested by direct current injection, with a firing frequency of 50–100 Hz. The duration of the 1st and last action potentials was statistically indistinguishable, 680 ± 26 *versus* 758 ± 38 μs ($n = 6$, $P > 0.1$).

Does DAP have the same characteristics in terminals and axons?

Traces in Fig. 5*A* show that the DAP at terminal varicosities has characteristics similar to those recorded in the main axon. In order to quantitatively compare DAP in the two locations, the magnitude of DAP was normalized as a fraction of action potential amplitude ($R_{DAP/AP}$) (Fig. 7*A*). DAP amplitude was measured from the baseline before the onset of the action potential to the minimal point of

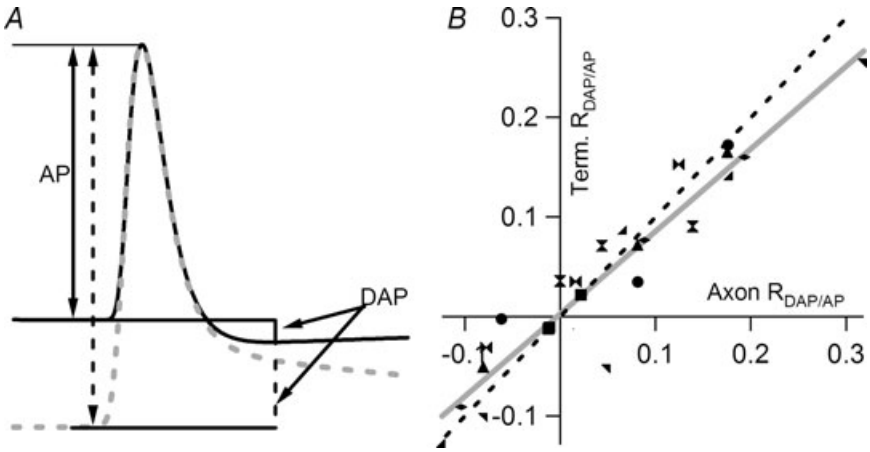

Figure 7. DAP amplitude and polarity co-vary in terminals and axons
A, quantification of DAP as the membrane potential is shifted. In order to compare results recorded form different preparations, DAP was normalized by the amplitude of the action potential, measured from the baseline to peak (AP). Using microelectrode-recorded E traces in the secondary axon as a common reference, the DAP was measured at the minimal point following an action potential fired from depolarized membrane potential (continuous line). The same time point was then used to measure DAP following an action potential fired from hyperpolarized membrane potential (grey dashed line). The same time point was also applied to the DAP measured from F traces recorded simultaneously. *B*, correlation between the $R_{DAP/AP}$ measured from terminals and axons. $R_{DAP/AP}$ measured from F traces significantly correlates with that recorded with the microelectrode in the axon. A linear fit has a slope of 0.83, which is significantly different from 1 ($P < 0.01$), and a correlation coefficient of 0.94, which is also significant ($P < 0.01$). The dashed straight line represents the 45 deg line. The plot was compiled from 8 preparations, each shown with a different symbol, and each preparation contributed 3 points, i.e. 3 membrane potential levels. The linear fit was applied to all 24 data points.

the inverted DAP of an E trace (Fig. 7*A*, continuous line). DAP amplitudes measured from resting or hyperpolarized potentials were also taken from this same time point. Thus, the amplitude was positive when DAP was depolarizing and negative when DAP was inverted. In each preparation, the DAP and AP measured from F traces used the same time point determined from the corresponding E trace. There was a linear correlation between $R_{DAP/AP}$ determined from terminals and that measured from axons (Fig. 7*B*). The linear fit of data points from eight preparations, each contributing three data points, exhibited a slope of 0.83 and a correlation coefficient of 0.94, which was highly significant (Fig. 7*B*, grey line). Thus, DAP amplitude and polarity covaried at the axon and terminal. The slope was close to, but significantly different from, 1 (Fig. 7*B*, dashed line). However, this does not automatically suggest that DAP, relative to action potential amplitude, is smaller in terminals than in axons. As discussed below, spatial decay based on cable properties may explain this slope of less than 45 deg.

Discussion

This report demonstrates the use of high resolution fluorescence recording of action potentials from fine axons and varicosities at the crayfish opener neuromuscular junction. Results indicated that action potential duration in terminal varicosities was significantly shorter than that recorded in the main axonal branches. A shift in resting membrane potential did not change the peak level of an action potential but did alter the amplitude measured from baseline to peak. The duration of an isolated spike was not modulated by shifting resting membrane potential. However, a slight prolongation of action potential was detectable when high frequency firing was initiated at depolarized membrane potential. Spike duration was not altered if high frequency firing was activated from resting or hyperpolarized membrane potential. At resting level, a prominent depolarizing after-potential (DAP) was observed in both the main axon and terminals and this DAP could be inverted (enlarged) at depolarized (hyperpolarized) membrane potential at both locations. Comparing the ratio of DAP amplitude to action potential amplitude between axon and terminals suggested that there was little spatial gradient in potential during DAP. Results in this report represent the first direct observation of electrophysiological activity at its release sites, although the crayfish opener preparation has a long history as a model system for synaptic transmission and plasticity.

Resolution of the voltage indicator

Data presented in this report were typically taken from a string of ∼5 varicosities within a circular region of 30–50 μm diameter. Recordings with finer spatial resolution should be possible if a sensor array were used, but difficulties may arise as a result of the low signal level in fine axons and individual varicosities. Indeed, the main difficulty when using voltage indicators is the small signal, ∼1% peak to peak for action potentials. With signal averaging, a resolution of 8–10 mV for high bandwidth signals was achieved here. Signal filtering or trace smoothing improved signal resolution by a factor of ∼2. Although further improvement in the signal may be possible, recordings shown in this report have already been optimized by selectively staining single axons and by imaging structures on the upper surface of the preparation.

Despite the great advantage of being able to monitor electrophysiological activity in the terminal, voltage indicator recordings do not provide reliable DC signals, mainly due to low signal levels and photobleaching. However, by correcting the bleaching trend, accurate recording of intracellular signals with a duration up to 200 ms should be possible; see the subthreshold responses in Fig. 3*Bb* for example. This time resolution is best suited for investigating synaptic and action potential interactions as opposed to slower events such as modulation mediated through G-proteins.

Until now, the main application of voltage indicators has been in time course analyses rather than investigation of absolute amplitude, because there is no direct means of calibrating the amplitude of fluorescence transients (Zecevic *et al.* 2003). In this report, action potential amplitude has been used as the calibrator (Zhou *et al.* 2007), based on the assumption that action potential amplitude reaches the same peak level at both main axonal branches and terminals. This calibration procedure and assumption could be refined in the future by incorporating cable modelling. Meanwhile, informative insights may be best gained by carefully designed protocols such that knowledge of absolute amplitude is not essential.

Electrophysiological activity in terminal varicosities

Direct measurement of electrophysiological events in presynaptic terminals is feasible in a limited number of preparations. Of these preparations, only mossy fibre terminals of the hippocampal CA3 region and terminals of the posterior pituitary have been analysed with the connecting axon fully in place. This structural integrity is important because fine connecting axons and varicosities may act as a current source and sink for each other and help shape action potential waveforms and excitability (Luscher & Shiner, 1990*a*). In the posterior pituitary, action potentials in axons exhibited shorter duration than those recorded in terminals (Bourque, 1991). In contrast, action potentials in mossy fibre varicosities have been shown to be briefer than those recorded in soma (Engel & Jonas, 2005). An analogous observation was made in this report, namely that action potential half-width in terminal

varicosities was narrower than that in the main branches of the axon. This shorter duration in terminals could be due to Ca^{2+}-activated K^+ channels suggested to be localized in terminal varicosities (Sivaramakrishnan *et al.* 1991). The observation that the falling phase of terminal and axonal action potentials coincided in time suggests that the repolarizing phase in the main branches may be shaped in part by the antidromic spread of activity from terminals. Thus, in the main branch, the rising phase and the peak of an action potential are probably determined by local Na^+ channels, while the falling phase may be shaped at least partially by the antidromic spread of the terminal action potential. In other words, it appears that whereas action potentials propagate forward, from the main branches to the terminals, the entire axonal arborization repolarizes together. These characteristics may act as a safeguard to prevent the reverberation of action potentials (Luscher & Shiner, 1990*a*,*b*).

The idea that the rising phase of an action potential is determined by local Na^+ channels may add insights to previous studies of presynaptic inhibition in this preparation. These studies have suggested that presynaptic inhibition involves a reduction in action potential amplitude at release sites, partly because bath-applied GABA reduced action potential amplitude recorded in the main branches (Baxter & Bittner, 1981; Blundon & Bittner, 1992; Parnas *et al.* 2000; DeMill & Delaney, 2005). However, although a reduction in action potential amplitude recorded in the main axon has been reported by stimulating the inhibitor (Baxter & Bittner, 1981; Parnas *et al.* 2000; DeMill & Delaney, 2005), this reduction has not been observed consistently (Blundon & Bittner, 1992; author's observations). Results reported here provide a possible explanation for the inconsistency. Specifically, changes in spike amplitude in terminals may not be detectable – because local Na^+ channels in the main branches may dominate the rising phase and peak of action potentials recorded with a microelectrode – unless the input resistance of the entire arborization is significantly reduced by bath-applied GABA.

The brief duration of action potentials in the terminals also has implications for the kinetic properties of presynaptic Ca^{2+} channels. The kinetics of Ca^{2+} channels in the presynaptic terminal are tuned to action potential duration. For example, at 37°C, individual action potentials in the calyx of Held and hippocampal CA1 mossy fibre terminals open ∼70–90% of Ca^{2+} channels (Borst & Sakmann, 1998; Geiger & Jonas, 2000; Bischofberger *et al.* 2002). (A single action potential at the squid giant synapse, in contrast, opens only about 10% of total Ca^{2+} channels; Llinás *et al.* 1981; Augustine, 1990). The rapid channel activation and resulting high percentage of channels opening under these conditions suggest that the increase in Ca^{2+} influx associated with spike broadening is mainly caused by the prolongation of channel opening, and that any increase in Ca^{2+} influx due to a larger number of open channels is insignificant (Bischofberger *et al.* 2002). Given the high Ca^{2+} cooperativity of the release process, small linear changes in Ca^{2+} influx in response to variations in action potential duration would be sufficient to result in significant changes in transmitter release (Schneggenburger & Neher, 2005). Estimates of Ca^{2+} influx using imaging techniques have shown a linear relationship between total Ca^{2+} influx and spike duration in this preparation (Vyshedskiy & Lin, 2000) with a normalized slope of ∼1, not unlike the correlations reported for the calyx of Held and mossy fibre terminals. The brief duration of terminal action potential and the linear correlation in total Ca^{2+} influx and action potential duration provide useful constraints towards inferring the properties of presynaptic Ca^{2+} channels.

Modulation of action potential waveform

It has been shown that shifting resting membrane potential can modulate transmitter output by altering the resting level of $[Ca^{2+}]$ (Awatramani *et al.* 2005) or by shaping the action potential waveform (Charlton & Bittner, 1978; Debanne *et al.* 1997; Shu *et al.* 2006). In the crayfish opener preparation, the resting membrane potential of presynaptic axons is modulated under physiological conditions, by serotonin acting through I_h (Beaumont & Zucker, 2000) and by enhanced sodium pump activity following high frequency firing (Wojtowicz & Atwood, 1985). In this report, the possible impact of shifting resting membrane potential on spike duration was examined in presynaptic terminals. Depolarizing or hyperpolarizing membrane potential by up to 20 mV did not significantly alter the duration of action potentials in the terminal varicosities, whereas the amplitude of terminal spikes varied with the resting level. This variation arose from the characteristic that the peak level of terminal action potential remained constant while its resting level was shifted. These observations held true even after I_h was activated by prolonged hyperpolarization, thereby reducing axonal input resistance, and after prolonged depolarization, thereby inactivating a significant fraction of Na^+ channels. Therefore, the density of terminal Na^+ channels is probably sufficiently high to ensure stable peak levels despite significant changes in input resistance or Na^+ channel inactivation.

Terminal action potential duration has been shown to lengthen during high frequency firing (Bourque, 1991; Jackson *et al.* 1991; Geiger & Jonas, 2000; see Debanne, 2004 for review). Such frequency-dependent modulation in axonal terminals could shape the magnitude of short-term plasticity. Although the crayfish opener preparation has been one of the classical model systems for studying paired-pulse facilitation (Zucker & Regehr, 2002), the

stability of spike duration at release sites has not been clearly established. Recordings shown in this report indicated no detectable change in terminal spike duration when the train was fired from resting level, although a slight prolongation was observed in the main axonal branches. However, high frequency firing at depolarized membrane potential resulted in a 23% prolongation of action potential duration. The specific mechanisms underlying this prolongation are unclear, but are likely to involve the accumulated inactivation of K^+ channels during the high frequency train. It should be noted that this conclusion is based on a relatively short train of 10 action potentials, and thus is most relevant to the paired pulse facilitation for which this preparation has been used extensively (Zucker & Regehr, 2002). It is possible that this frequency-dependent modulation would be more apparent if the train were to persist longer and fire more action potentials (Bourque, 1991; Jackson *et al.* 1991; Geiger & Jonas, 2000).

The functional consequences of frequency-dependent modulation remain to be fully explored. For example, it is unknown whether the 23% increase in action potential duration could significantly enhance Ca^{2+} influx. Although there was no clear change in spike duration when an action potential burst was fired from hyperpolarized membrane potential, the amplitude of the first spike was significantly greater than the amplitude of those that followed it (see also Charlton & Bittner, 1978). It is unclear how such a difference in action potential amplitude would affect presynaptic Ca^{2+} influx during a high frequency train.

Spatial distribution of the DAP and its function

Fluorescence transients recorded from terminals indicate that the depolarizing after-potential (DAP), initially reported in vertebrate myelinated axons (Barrett & Barrett, 1982), exists in the entire axonal arborization of the crayfish opener preparation. The origin of this potential in myelinated axons appears to be a combination of current discharge through perinodal leakage, persistent opening of Na^+ channels and perhaps M-current (Barrett & Barrett, 1982; David *et al.* 1995; McIntyre *et al.* 2002; Vervaeke *et al.* 2006). In addition, given the abundance of K^+ channels in axon terminals (Tabti *et al.* 1989), it is not surprising that K^+ conductance has been shown to shape the DAP time course (Morita & Barrett, 1990; David *et al.* 1995). The mechanism underlying this after-potential in the crayfish opener preparation has not been examined, although it has been suggested to be related to K^+ conductance with E_K being more depolarized than at resting level (Wojtowicz & Atwood, 1984). The functional significance of DAP is not fully understood. An initial modelling study based on myelinated axons suggested that DAP may be larger in terminals than in axons (Barrett & Barrett, 1982) but results shown here suggest that this cannot be the case at the crayfish opener preparation. In fact, the fractional amplitude of DAP in the terminals appears to be smaller than that in axons, given the slope of 0.83 shown in Fig. 7*B*. However, there are good reasons to believe that DAP amplitude is similar between axon and terminals when measured from resting membrane potential. In the plot shown in Fig. 7*B*, DAP amplitude was manipulated by shifting resting membrane potential through axonal current injection. Due to the cable properties of the axon, the shift in resting level in terminals would be less than that in the axon. As a result, the change in the driving force for DAP in the terminals should also be less, resulting in a smaller change in DAP amplitude. Since the reversal potential for DAP is slightly above resting membrane level, a difference of a few millivolts in resting level between axon and terminals would result in a relatively large change in the DAP driving force and amplitude. In contrast, the same small difference in resting level would have relatively small impact on action potential amplitude. As a result, $R_{DAP/AP}$ would appear to be smaller in terminals than in axon because of a significantly smaller driving force for the DAP. Thus, it is likely that there is no or little spatial gradient in potential during DAP. The time course of DAP has been correlated with a brief period of superexcitability following individual action potentials and consequently assumed to play a role in the regulation of axonal excitability (Barrett & Barrett, 1982; McIntyre *et al.* 2002). Results shown here suggest another function of DAP, namely that it keeps the action potential initiation level near the DAP reversal potential during high frequency bursts. Thus, DAP could help maintain the stability of action potential initiation and propagation during high frequency bursts even when resting membrane potential is changed under physiological conditions.

Results in this report show that although electrophysiological properties are in many respects similar in terminals and main axons, there are also important differences, chief among them being the duration of action potentials. Given its unique combination of technical advantages, the crayfish opener preparation may lend further insights to the understanding of axonal signal processing. Quantitative cable modelling, incorporating morphological details and passive responses, will be necessary to provide a more comprehensive description of this system.

References

Augustine GJ (1990). Regulation of transmitter release at the squid giant synapse by presynaptic delayed rectifier potassium current. *J Physiol* **431**, 343–364.

Awatramani GB, Price GD & Trussell LO (2005). Modulation of transmitter release by presynaptic resting potential and background calcium levels. *Neuron* **48**, 109–121.

Baccus SA (1998). Synaptic facilitation by reflected action potentials: enhancement of transmission when nerve impulses reverse direction at axon branch points. *Proc Natl Acad Sci U S A* **95**, 8345–8350.

Barrett EF & Barrett JN (1982). Intracellular recording from vertebrate myelinated axons: mechanism of the depolarizing afterpotential. *J Physiol* **323**, 117–144.

Baxter DA & Bittner GD (1981). Intracellular recordings from crustacean motor axons during presynaptic inhibition. *Brain Res* **223**, 422–428.

Beaumont V & Zucker RS (2000). Enhancement of synaptic transmission by cyclic AMP modulation of presynaptic I_h channels. *Nat Neurosci* **3**, 133–141.

Bischofberger J, Geiger JR & Jonas P (2002). Timing and efficacy of Ca^{2+} channel activation in hippocampal mossy fiber boutons. *J Neurosci* **22**, 10593–10602.

Blundon JA & Bittner GD (1992). Effects of ethanol and other drugs on excitatory and inhibitory neurotransmission in the crayfish. *J Neurophysiol* **67**, 576–587.

Borst JG & Sakmann B (1998). Calcium current during a single action potential in a large presynaptic terminal of the rat brainstem. *J Physiol* **506**, 143–157.

Bourque CW (1991). Activity-dependent modulation of nerve terminal excitation in a mammalian peptidergic system. *Trends Neurosci* **14**, 28–30.

Cattaert D, Libersat F & El Manira AA (2001). Presynaptic inhibition and antidromic spikes in primary afferents of the crayfish: a computational and experimental analysis. *J Neurosci* **21**, 1007–1021.

Charlton MP & Bittner GD (1978). Presynaptic potentials and facilitation of transmitter release in the squid giant synapse. *J Gen Physiol* **72**, 487–511.

Cox CL, Denk W, Tank DW & Svoboda K (2000). Action potentials reliably invade axonal arbors of rat neocortical neurons. *Proc Natl Acad Sci U S A* **97**, 9724–9728.

David G, Modney B, Scappaticci KA, Barrett JN & Barrett EF (1995). Electrical and morphological factors influencing the depolarizing after-potential in rat and lizard myelinated axons. *J Physiol* **489**, 141–157.

Debanne D (2004). Information processing in the axon. *Nat Rev Neurosci* **5**, 304–316.

Debanne D, Guerineau NC, Gahwiler BH & Thompson SM (1997). Action-potential propagation gated by an axonal I_A-like K^+ conductance in hippocampus. *Nature* **389**, 286–289.

DeMill CM & Delaney KR (2005). Interaction between facilitation and presynaptic inhibition at the crayfish neuromuscular junction. *J Exp Biol* **208**, 2135–2145.

Dixon D & Atwood HL (1985). Crayfish motor nerve terminal's response to serotonin examined by intracellular microelectrode. *J Neurobiol* **16**, 409–424.

Djurisic M, Antic S, Chen WR & Zecevic D (2004). Voltage imaging from dendrites of mitral cells: EPSP attenuation and spike trigger zones. *J Neurosci* **24**, 6703–6714.

Dudel J & Kuffler SW (1961). Presynaptic inhibition at the crayfish neuromuscular junction. *J Physiol* **155**, 543–562.

Dudel J, Parnas I & Parnas H (1983). Neurotransmitter release and its facilitation in crayfish muscle. VI. Release determined by both, intracellular calcium concentration and depolarization of the nerve terminal. *Pflugers Arch* **399**, 1–10.

Engel D & Jonas P (2005). Presynaptic action potential amplification by voltage-gated Na^+ channels in hippocampal mossy fiber boutons. *Neuron* **45**, 405–417.

Geiger JR & Jonas P (2000). Dynamic control of presynaptic Ca^{2+} inflow by fast-inactivating K^+ channels in hippocampal mossy fiber boutons. *Neuron* **28**, 927–939.

Grossman Y, Parnas I & Spira ME (1979). Differential conduction block in branches of a bifurcating axon. *J Physiol* **295**, 283–305.

Gu XN (1991). Effect of conduction block at axon bifurcations on synaptic transmission to different postsynaptic neurones in the leech. *J Physiol* **441**, 755–778.

Jackson MB, Konnerth A & Augustine GJ (1991). Action potential broadening and frequency-dependent facilitation of calcium signals in pituitary nerve terminals. *Proc Natl Acad Sci U S A* **88**, 380–384.

Koester HJ & Sakmann B (2000). Calcium dynamics associated with action potentials in single nerve terminals of pyramidal cells in layer 2/3 of the young rat neocortex. *J Physiol* **529**, 625–646.

Leao RM, Kushmerick C, Pinaud R, Renden R, Li GL, Taschenberger H, Spirou G, Levinson SR & von Gersdorff H (2005). Presynaptic Na^+ channels: locus, development, and recovery from inactivation at a high-fidelity synapse. *J Neurosci* **25**, 3724–3738.

Llinás R, Steinberg IZ & Walton K (1981). Presynaptic calcium currents in squid giant synapse. *Biophys J* **33**, 289–321.

Luscher HR & Shiner JS (1990*a*). Computation of action potential propagation and presynaptic bouton activation in terminal arborizations of different geometries. *Biophys J* **58**, 1377–1388.

Luscher HR & Shiner JS (1990*b*). Simulation of action potential propagation in complex terminal arborizations. *Biophys J* **58**, 1389–1399.

MacDermott AB, Role LW & Siegelbaum SA (1999). Presynaptic ionotropic receptors and the control of transmitter release. *Annu Rev Neurosci* **22**, 443–485.

McIntyre CC, Richardson AG & Grill WM (2002). Modeling the excitability of mammalian nerve fibers: influence of afterpotentials on the recovery cycle. *J Neurophysiol* **87**, 995–1006.

Matveev V, Zucker RS & Sherman A (2004). Facilitation through buffer saturation: constraints on endogenous buffering properties. *Biophys J* **86**, 2691–2709.

Mejia-Gervacio S & Marty A (2006). Control of interneurone firing pattern by axonal autoreceptors in the juvenile rat cerebellum. *J Physiol* **571**, 43–55.

Morita K & Barrett EF (1990). Evidence for two calcium-dependent potassium conductances in lizard motor nerve terminals. *J Neurosci* **10**, 2614–2625.

Palmer LM & Stuart GJ (2006). Site of action potential initiation in layer 5 pyramidal neurons. *J Neurosci* **26**, 1854–1863.

Parnas I, Rashkovan G, Ravin R & Fischer Y (2000). Novel mechanism for presynaptic inhibition: $GABA_A$ receptors affect the release machinery. *J Neurophysiol* **84**, 1240–1246.

Pouzat C & Marty A (1999). Somatic recording of GABAergic autoreceptor current in cerebellar stellate and basket cells. *J Neurosci* **19**, 1675–1690.

Schneggenburger R & Neher E (2005). Presynaptic calcium and control of vesicle fusion. *Curr Opin Neurobiol* **15**, 266–274.

Shu Y, Hasenstaub A, Duque A, Yu Y & McCormick DA (2006). Modulation of intracortical synaptic potentials by presynaptic somatic membrane potential. *Nature* **441**, 761–765.

Sivaramakrishnan S, Bittner GD & Brodwick MS (1991). Calcium-activated potassium conductance in presynaptic terminals at the crayfish neuromuscular junction. *J Gen Physiol* **98**, 1161–1179.

Smith DO (1980). Mechanisms of action potential propagation failure at sites of axon branching in the crayfish. *J Physiol* **301**, 243–259.

Soleng AF, Chiu K & Raastad M (2003). Unmyelinated axons in the rat hippocampus hyperpolarize and activate an H current when spike frequency exceeds 1 Hz. *J Physiol* **552**, 459–470.

Tabti N, Bourret C & Mallart A (1989). Three potassium currents in mouse motor nerve terminals. *Pflugers Arch* **413**, 395–400.

Vervaeke K, Gu N, Agdestein C, Hu H & Storm JF (2006). Kv7/KCNQ/M-channels in rat glutamatergic hippocampal axons and their role in regulation of excitability and transmitter release. *J Physiol* **576**, 235–256.

Vyshedskiy A & Lin JW (2000). Presynaptic Ca^{2+} influx at the inhibitor of the crayfish neuromuscular junction: a photometric study at a high time resolution. *J Neurophysiol* **83**, 552–562.

Wilke RA, Ahern GP & Jackson MB (1998). Membrane excitability in the neurohypophysis. *Adv Exp Med Biol* **449**, 193–200.

Wojtowicz JM & Atwood HL (1984). Presynaptic membrane potential and transmitter release at the crayfish neuromuscular junction. *J Neurophysiol* **52**, 99–113.

Wojtowicz JM & Atwood HL (1985). Correlation of presynaptic and postsynaptic events during establishment of long-term facilitation at crayfish neuromuscular junction. *J Neurophysiol* **54**, 220–230.

Zecevic D, Djurisic M, Cohen LB, Antic S, Wachowiak M, Falk CX & Zochowski MR (2003). Imaging nervous system activity with voltage-sensitive dyes. *Curr Protoc Neurosci* Chap. 6, Unit 6.17.

Zhou WL, Yan P, Wuskell JP, Loew LM & Antic SD (2007). Intracellular long-wavelength voltage-sensitive dyes for studying the dynamics of action potentials in axons and thin dendrites. *J Neurosci Methods* **164**, 225–239.

Zucker RS (1974*a*). Crayfish neuromuscular facilitation activated by constant presynaptic action potentials and depolarizing pulses. *J Physiol* **241**, 69–89.

Zucker RS & Regehr WG (2002). Short-term synaptic plasticity. *Annu Rev Physiol* **64**, 355–405.

Acknowledgements

I thank Nicky Schweitzer for correcting my English. This work is supported by National Institutes of Health Grant NS31707.

Supplemental material

Online Supplemental material for this paper can be accessed at: http://jp.physoc.org/cgi/content/full/jphysiol.2008.158089/DC1